Korean J. Chem. Eng., **27**(2), 609-618 (2010)
DOI: 10.1007/s11814-010-0078-x

Modeling and simulation of a simulated moving bed for adsorptive para-xylene separation

Jinsuk Lee*, Nam Cheol Shin*, Youngsub Lim, and Chonghun Han**,†**

*Samsung Total, 411-1, Dokgod-Ri, Daesan-Up, Seosan-Si, Chungnam 356-711, Korea
**School of Chemical and Biological Engineering, Seoul National University, Seoul 151-744, Korea
(*Received 27 April 2009 • accepted 18 August 2009*)

Abstract−A multi-cell model was developed to analyze the behavior of a simulated moving bed process for adsorptive para-xylene separation from other xylene isomers. A novel technology for a semi-batch mode adsorption experiment was developed and used for fast and accurate data collection. Interaction parameters between different species for a multi-component extended Langmuir isotherm were estimated from single and multi-component adsorption experiments and implemented into the model. The parameters such as porosities, particle density and mass transfer coefficients were obtained from adsorbent analysis and commercial plant operation. To resolve the problem of high dimensionality, a cell-by-cell approach was proposed to solve the model. The recovery and purity of para-xylene as well as the concentration profile calculated from the model were in good agreement with the actual data. The effects of channeling and feed composition change were simulated, and they turned out to be physically meaningful. The simulation model will be used for operation condition optimization, trouble shooting, and productivity enhancement including a configuration change.

Key words: Adsorptive Para-xylene Separation, SMB (Simulated Moving Bed), Parex, Multi-cell Model, Cell-by-cell Approach

INTRODUCTION

PX (para-xylene) is one of the most important petrochemical products in use today. It is used as a raw material for making terephthalic acid, which is used in the production of polyesters and polyethylene terephtalates. The average annual growth rate for the use of PX is expected to be 6% for the next decade [1]. The main sources of PX and other xylene isomers in the petrochemical industry are naphtha reforming in an aromatics complex and pygas (pyrolysis gasoline) cut from naphtha cracking. Fig. 1 shows a typical aromatics complex which consists of naphtha prefractionation and hydrotreating, CCR (continuous catalyst regeneration) reforming, xylene fractionation, aromatics extraction and benzene/toluene fractionation, transalkylation and disproportionation, xylene isomerization and PX separation.

Because of their close boiling points, xylene isomers, PX, MX, OX and EB, cannot be practically separated by a conventional distillation unit. The first separation processes were based on the solvent extraction or crystallization. Since 1971, when UOP commercialized the first Parex unit, the simulated moving bed (SMB) adsorptive separation process has emerged as a superior technology [2-4]. SMB was developed to mimic a TMB (true moving bed) by switching the positions of the ports for the feed inlet and product outlet. Port switching has an effect that is similar to the way that TMB behaves, where the adsorbent solid countercurrently circulates along the bed axis in the opposite direction of the liquid flow as TMB behaves.

†To whom correspondence should be addressed.
E-mail: chhan@snu.ac.kr

In spite of some new versions of SMB recently released [5-9], the classical four-zone SMB is still most widely used in industry. Usually, desorbent comes out of the SMB with both the extract and raffinate and is later separated by distillation columns as depicted in Fig. 2 [10]. All of the transfer lines connecting the rotary valves and adsorbent beds are shared by the inlet and outlet streams. Therefore, the transfer lines should be contaminated by the other stream unless an appropriate action is taken. To prevent the extract stream from being contaminated by mixed xylene, the Parex unit has internal and external line flushing sequences added to the conventional four-zone SMB port switching, which increases the total number of zones to seven. This makes an the analysis of the Parex process much more difficult and leads us to rely only on operation experience.

Even though several studies on the modeling, simulation or optimization of a Parex unit have been done [11-19], the application to a real commercial plant is hardly found elsewhere because of its nonideal configuration including dead volume. The dead volume of a real Parex unit comes mainly from the transfer lines connecting the rotary valve and adsorbent beds, the void between beds, and the pipes and pumps belonging to the recirculation line. Studies on the effect of this dead volume on the SMB process are quite rare. Azevedo et al. showed that the dead volume of the recirculation line affected the performance of the Parex process [11]. Migliorini et al. assessed the effect of the dead volume between column beds in a lab-scale SMB unit [15]. Minceva and Rodrigues studied the dead volume effect of the transfer line from rotary valve to adsorbent beds on the separation performance of the Parex process [16,17]. However, a study considering the effect of all of the dead volume elements synthetically to a real commercial plant is hardly found. The lack of an appropriate adsorption isotherm is another factor

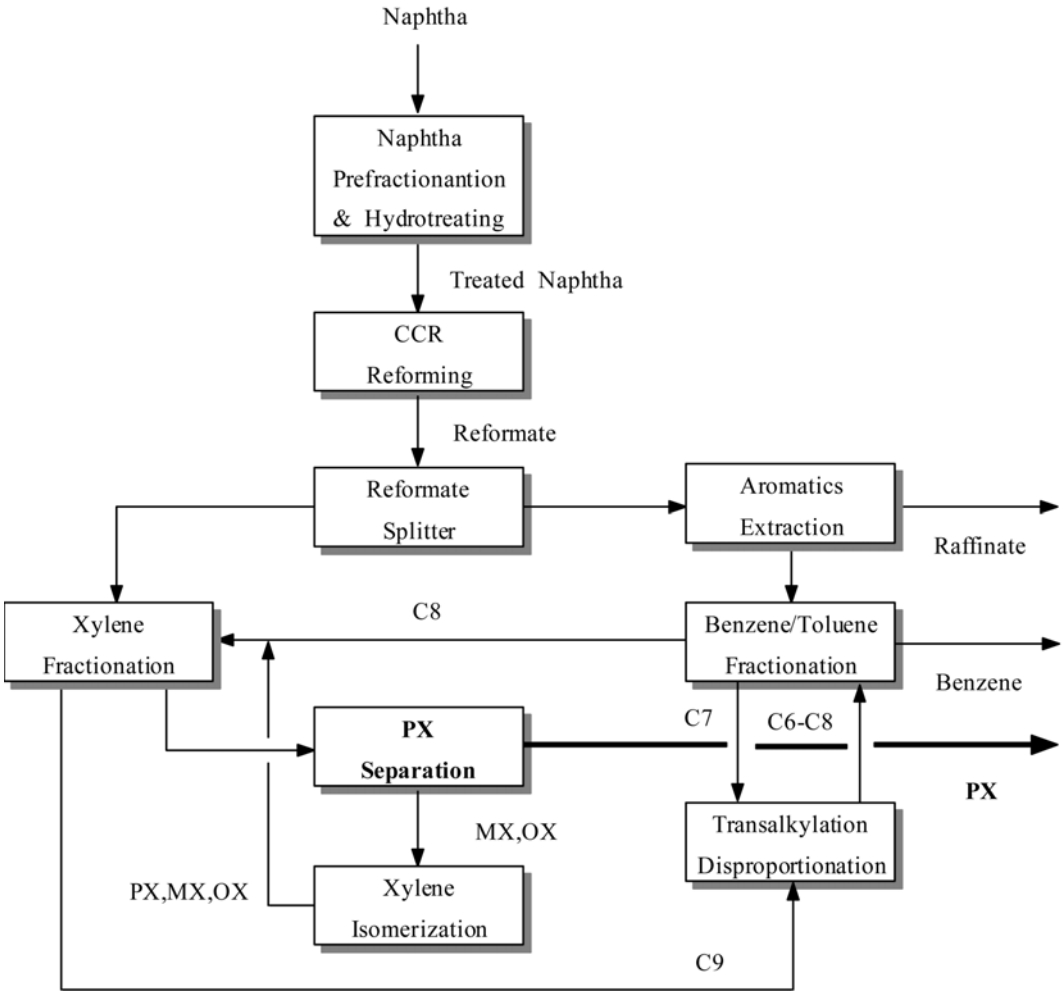

Fig. 1. Simplified process diagram of typical aromatics complex.

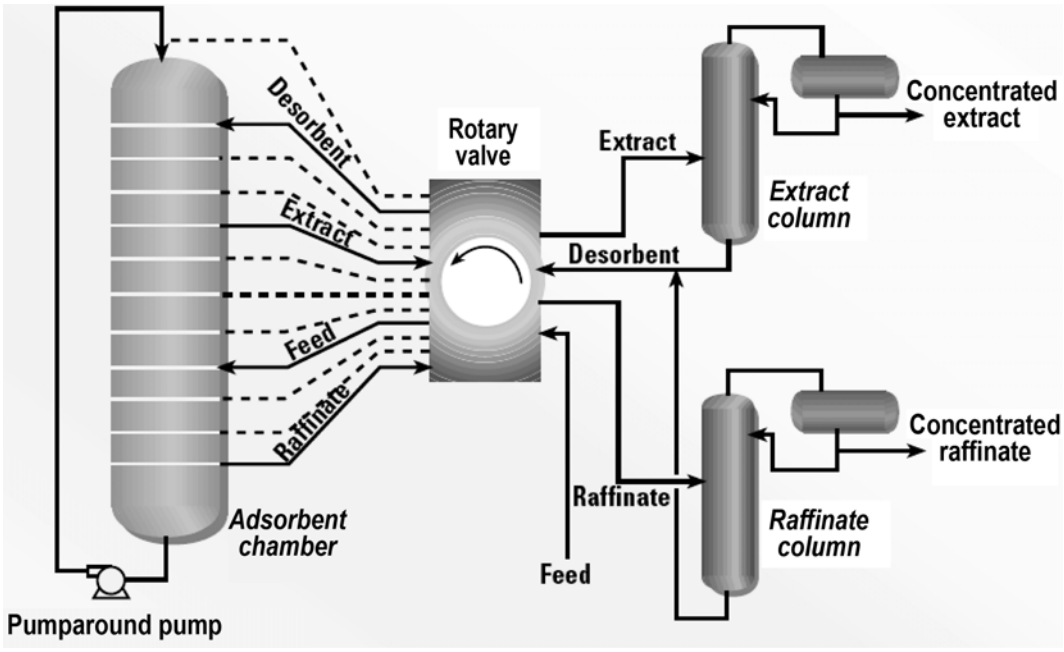

Fig. 2. Schematic diagram of Parex process.

making the simulation of a real Parex unit difficult. Because of the multi-component system of the real process, the adsorption behavior cannot be predicted by simple extended versions of single component isotherm equations. This nonideality may be due to the interaction between different adsorbed species which was discussed in the Fowler isotherm equation by using interaction parameters for gas phase adsorption [20]. We obtained the interaction parameters from the adsorption experiment, and applied this to a multi-component system isotherm.

The objective of this study was to present a more detailed model of the SMB process for PX separation. The effect of all of the dead volume elements was reflected in the model synthetically. In particular, the effect caused by channeling on the separation performance was elucidated. A liquid phase multi-component adsorption isotherm with interaction parameters reflecting nonideality was also suggested. The results of this study have already contributed to more economical industrial operations.

MATHEMATICAL MODEL

A Parex unit consists of 24 beds with two individual chambers that each contain 12 beds. Therefore, in order to construct a mathematical model a single bed has to be modeled and combined with other bed models. A schematic diagram for a single bed is shown

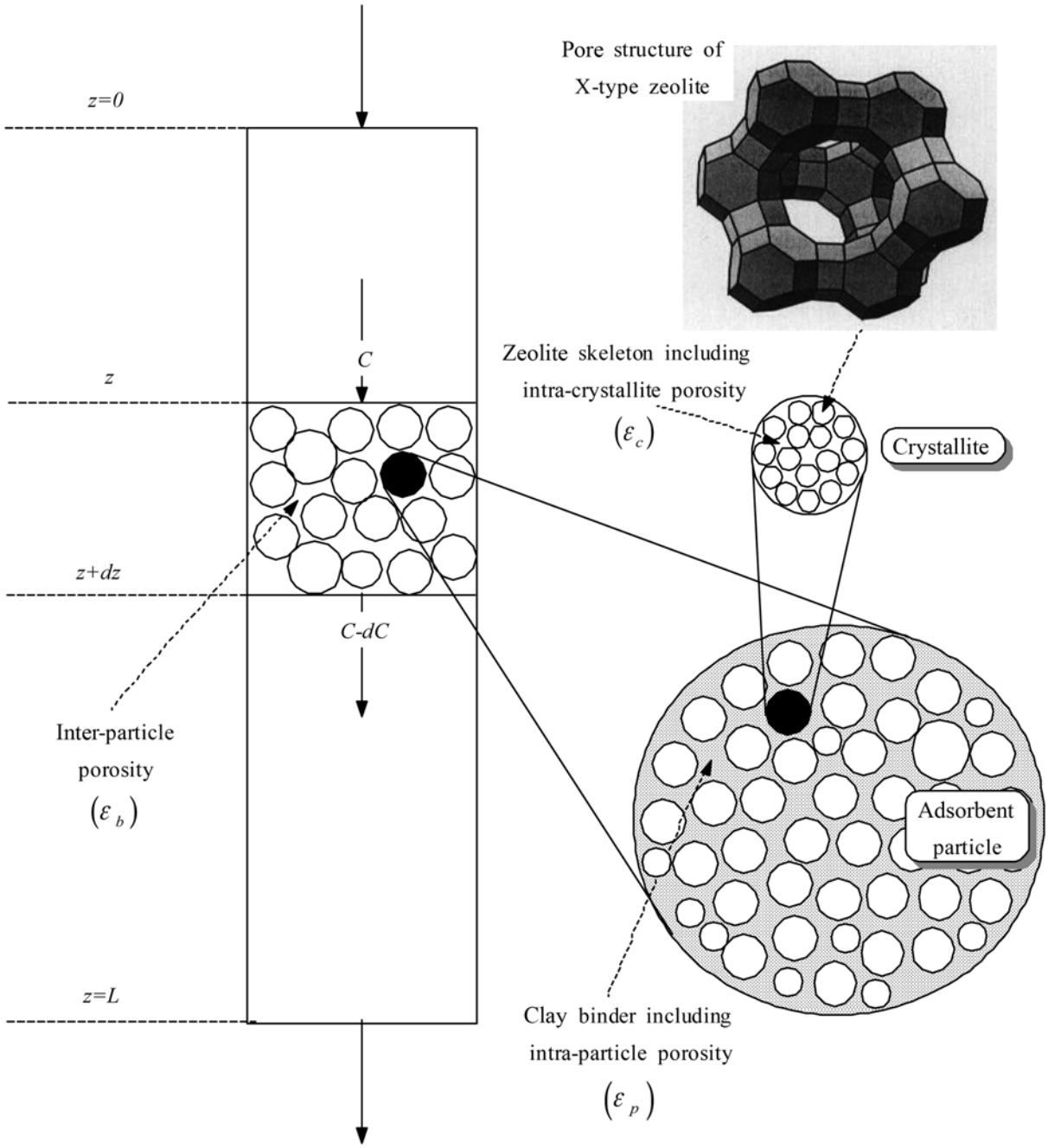

Fig. 3. Schematic diagram showing a single bed.

in Fig. 3.

The mass balances of a bed slice lead to PDEs (partial differential equations). With a linear driving force approximation to simplify the problem as proposed by Glueckauf and Coates, the following PDEs with appropriate boundary and initial conditions can be derived [21-23].

$$\frac{\partial C_{l,i}}{\partial t} - D_{L,i}\frac{\partial^2 C_{l,i}}{\partial z^2} + v\frac{\partial C_{l,i}}{\partial z} + \frac{1-\varepsilon_t}{\varepsilon_t}\frac{\partial q_i}{\partial t} = 0 \quad (1)$$

$$\frac{\partial q_i}{\partial t} = k_i(q_i^* - q_i) \quad (2)$$

$$q_i = f(C^*'s, q^*'s) \quad (3)$$

A multi-cell model with two phases (free liquid and adsorbed liquid phases) in each cell was proposed and developed as was done similarly by other researchers [24,25]. Each bed was divided into numerous cells to quantify the degree of axial dispersion. The number of cells was determined to be 16 by dividing the bed height by HETP, which can be calculated by van Deemter's equation [26].

As illustrated in Fig. 4, the total volume of a cell was once again divided into two parts: free liquid and adsorbed liquid phases. The volume fraction of the free liquid phase is ε_t and that of the adsorbed liquid phase is $(1-\varepsilon_b)(1-\varepsilon_p)\varepsilon_c$, where ε_c is the crystallite porosity. The remaining portion corresponds to the solid phase and need not be considered in the model. Considering that the molecular diameters of PX, MX and OX are 5.9 Å, 6.3 Å, and 6.6 Å, respectively [27] and that the pore size of X-type zeolite is about 8 Å [28] the assumption of such a volume division seems to be reasonable.

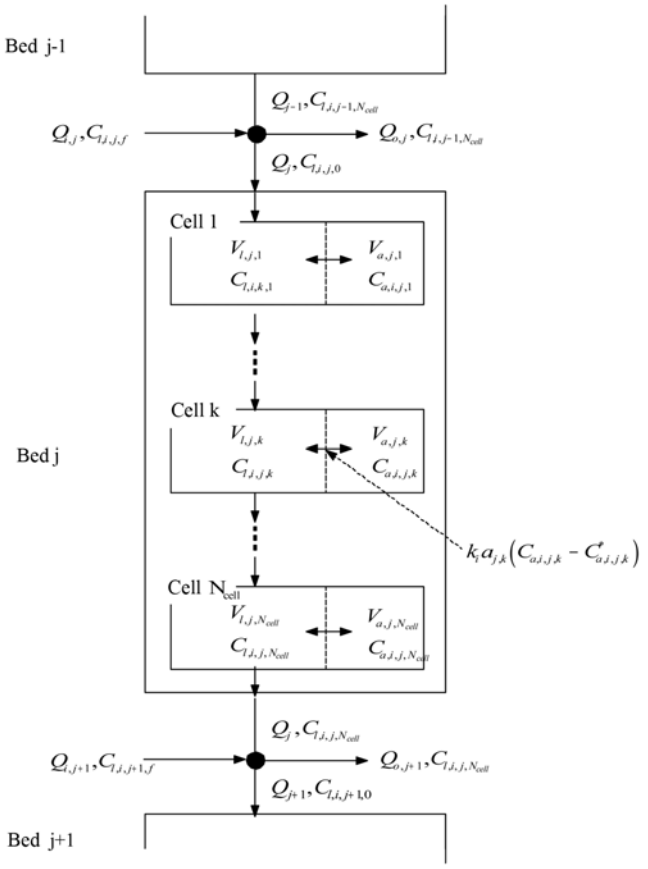

Fig. 4. Conceptual diagram of multi-cell model.

The mass balance equations for the *i*-th species in each phase of the *k*-th cell belonging to the *j*-th bed can be derived as follows:

$$V_{l,j,k}\frac{dC_{l,i,j,k}}{dt} = Q_jC_{l,i,j,k-1} - Q_jC_{l,i,j,k} - k_ia_{j,k}(C^*_{a,i,j,k} - C_{a,i,j,k}) \quad (6)$$

$$V_{a,j,k}\frac{dC_{a,i,j,k}}{dt} = k_ia_{j,k}(C^*_{a,i,j,k} - C_{a,i,j,k}) \quad (7)$$

Here, the subscripts i, j, k, *l*, a on C or V denote the species number, bed number, cell number, free liquid phase, and adsorbed liquid phase, respectively. As shown in Eq. (7), the adsorbed liquid phase is assumed to have only mass transfer and no forced convectional flow. From the simple mass balance at the node between the beds, the feed concentration into the first cell (k=1) of the j-th bed can be expressed as follows:

$$C_{l,i,j,0} = \frac{Q_{j-1}C_{l,i,j-1,N_{cell}} + Q_{i,j}C_{l,i,j,f} - Q_{o,j}C_{l,i,j-1,N_{cell}}}{Q_j} \quad (8)$$

The cell number of the last cell should be N_{cell} which is designated as the total number of cells per bed. Q_i and Q_o can be zero if the node does not correspond to the inlet and outlet nodes, respectively. The relationship between the mass and volume based equilibrium concentration of the adsorbed species, q^* and C^*_a, can be expressed as follows:

$$q_i^* = \frac{C^*_{a,i}\varepsilon_c(1-\varepsilon_p)}{\rho_p} \quad (9)$$

At each cell we define the selectivity of each component with respect to PX as follows:

$$S_i = \frac{q^*_{m,i}K_i}{q^*_{m,PX}K_{PX}} \quad (10)$$

Finally, we solve the following algebraic equations to get the concentrations at both the adsorbed and liquid phases.

$$\sum_j C^*_{a,j} = \rho_l \quad (11)$$

$$\frac{C^*_{a,PX}}{C^*_{l,PX}} = \frac{1}{S_i}\cdot\frac{C^*_{a,i}}{C^*_{l,i}} \quad (12)$$

ODEs (ordinary differential equations) (6) and (7) with algebraic Eqs. (8)-(12) were integrated numerically using the Gear method [29]. To obtain equilibrium concentrations, (11) and (12) were solved numerically using the Newton-Raphson method [30]. The dimension of the model differs considerably, based on the number of cells per bed. To avoid the problem of high dimensionality, a cell-by-cell approach was proposed. In the case of a cell-by-cell approach, since only a single cell is always solved, the total number of equations is reduced to 10. Here we briefly describe the calculation procedure of the cell-by-cell approach as follows:

◆ A certain cell is solved first during a certain short period of time (e.g. t_1 to $t_1+\Delta t$) and then the outlet concentrations from that cell are transferred to the next cell.

◆ The next cell is once again solved during the same period of time.

If the next cell belongs to the next bed, a feed concentration calculation using (8) is performed before integration.

◆ The whole integration from t_1 to $t_1+\Delta t$ is completed when we get back to the first cell again.

◆ Then the same procedure is repeated again from $t_1+\Delta t$ to $t_1+2\Delta t$. If the switching time is reached, every inlet and outlet port advances to the next bed before integration.

◆ If the difference in the concentration profile remains within the tolerance limit, it is assumed that the cyclic steady state has been reached. After several cycles (about 10-20) a cyclic steady state can be reached.

The program for performing the entire procedure was written in FORTRAN (Digital Visual Fortran) code. The user interface was written in Visual Basic to make the approach easier for engineers.

EXPERIMENTS

The adsorbent used in the experiments was X-type zeolite obtained from the open market since the adsorbents used in the Parex process are known to be X-type zeolite exchanged with K and Ba. Like other zeolites, the adsorption performance of this type of zeolite is very sensitive to water content [31]. Therefore, the water content was carefully controlled prior to the adsorption experiment. To keep the water content at the level for a commercial plant, the adsorbent was dried in an oven for about 24 hours and kept in a glove box to prevent additional water adsorption. The water content was measured by LOI (loss on ignition) at 900 °C.

The physical properties of the adsorbent that were needed in the simulation model were porosities and densities. After some mixed porosities were measured, bulk density and particle density, three porosities (ε_b, ε_p, ε_c) were calculated, as shown in the following three equations.

$$\varepsilon_b+(1-\varepsilon_b)\varepsilon_p=\text{known} \tag{13}$$

$$(1-\varepsilon_b)(1-\varepsilon_p)\varepsilon_c=\text{known} \tag{14}$$

$$\frac{\rho_{bulk}}{\rho_p}=\frac{\dfrac{(1-\varepsilon_b)m_{ads}}{N_p}}{\dfrac{\sum_i V_{ads,i}}{\dfrac{m_{ads}}{N_p}}}=(1-\varepsilon_b) \tag{15}$$

Semi-batch and batch adsorption experiments were conducted to get the adsorption isotherms for single and binary components, respectively, at a temperature and pressure that were similar to those in a commercial plant (177 °C and about 10 atm). Basically, the absolute value of pressure was not important in this system once it was high enough to keep the mixture of xylene and diluent in the liquid phase. The species considered are TOL and PDEB, as well as xylene isomers. Fig. 5 shows a schematic diagram of the experimental adsorption apparatus.

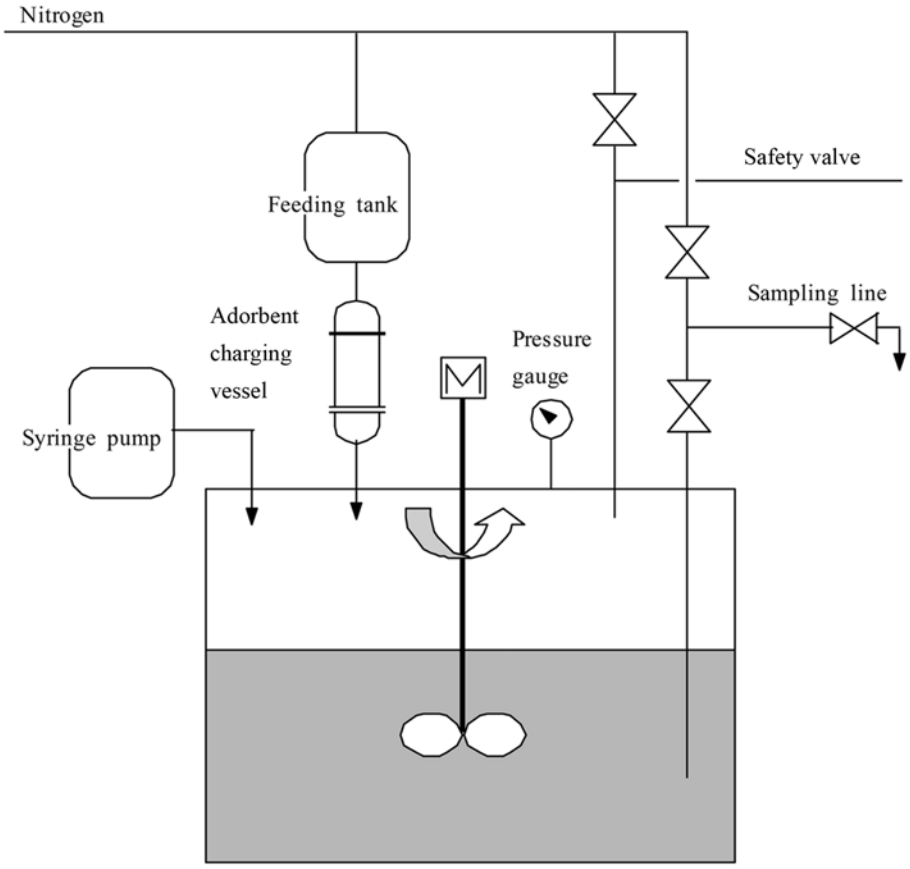

Fig. 5. Schematic diagram of the experimental apparatus.

Adsorbent was charged into an adsorbent charging vessel in the glove box to prevent water adsorption prior to the experiment. N-heptane, which has been confirmed to be an inert liquid, was used as a diluent to control xylene concentration at an appropriate level. A liquid sample was taken from the autoclave by a specially designed sampling line that was equipped with a nitrogen back blowing line to remove any liquid residue remaining in it.

The liquid sample was analyzed using an HP 5890 II GC (gas chromatography) with an HP-FFAP column (polyethylene glycol-TPA modified). Adsorption equilibrium was reached within 3 hours when the agitation speed was 650 rpm (revolutions per minute). The agitation speed was determined from a mixing test using a transparent beaker of a size similar to that the autoclave. Adsorbent particles were observed not to be broken after the experiment.

The concentrations of the adsorbed phase are also calculated from simple mass balance equations as follows.

$$q_i^* = \frac{V_{l,0}C_{l,i,0} - V_l C_{l,i}^*}{m_{ads}} \tag{16}$$

$$C_{l,i}^* = \frac{m_{l,i}}{V_l} = \frac{w_i \sum_j m_{l,j}}{V_l} \tag{17}$$

$$V_l = \frac{m_l}{\rho_l} = m_l \sum_j \frac{w_j}{\rho_{l,j}} \tag{18}$$

$$m_l = \sum_j m_{l,j} = \sum_j m_{l,j,0} - m_{ads} \sum_j q_j \tag{19}$$

Here w_i denotes the mass fraction of species i. The procedure to calculate the concentration of the adsorbed phase is as follows:

- Assume Σq_j^*.
- Calculate m_l, V_l and $C_{l,i}^*$ using (19), (18) and (17), respectively.
- Calculate q_i^* and Σq_j^* using (16).
- Check that the difference between the calculated and assumed Σq_j^* is within the tolerance. If not, repeat the procedure again.

Among the various isotherms tested including Langmuir [32] modified Langmuir [33] Freundlich [34] Sips [35] and Redlich-Peterson [36], all of the isotherms except Freundlich showed excellent agreement with the experimental data, resulting in a coefficient of determination (r^2) higher than 99%. Fig. 6 and Table 1 shows the experimental data with the Langmuir isotherm correlated, and parameters by regression of this data, respectively.

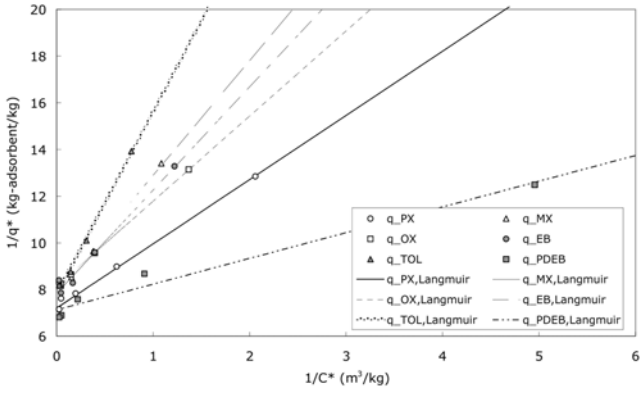

Fig. 6. Equilibrium concentrations of free liquid and adsorbed liquid phase for single component adsorption with Langmuir isotherm plotted and compared with the experimental data.

Table 1. Parameters in the Langmuir model by regression of the experimental data

	PX*	MX	OX	EB	TOL	PDEB
q_{max}^* (kg/kg-ads)	0.139	0.125	0.123	0.128	0.128	0.140
K (m^3/kg)	2.621	1.623	2.234	1.774	0.998	6.473

If the adsorption system considered is ideal there is no need for a multi-component experiment. After conducting some binary adsorption experiments we found that the xylene mixture system was not ideal. The IAST (ideal adsorbed solution theory) proposed by Myers and Prausnitz is known to be very useful in predicting multi-component adsorption behavior from a single component isotherm for gas systems and dilute liquid systems [37]. However, it is not applicable to liquid systems. Therefore we conducted binary experiments for every pair of the species being considered, with initial composition variation. Fowler and Guggenheim proposed modified equilibrium constants by multiplying an exponential term where interaction parameters multiplied by site fractions are included [20]. Considering the physical similarities, we adjusted the equilibrium constants to reflect the effect of other species by multiplying interaction parameters by the adsorbed phase equilibrium concentration, q^*. An example of the interaction parameters used for the Langmuir isotherm can be expressed as follows:

$$q_i^* = \frac{q_{m,i} K_i C_i^*}{1 + \sum_i K_i C_j^*} \tag{25}$$

$$K_i = K_{i,0} \exp\left(-\sum_j \omega_{ij} q_j^*\right) \tag{26}$$

All of the interaction parameters, ω's, that best fit the binary experimental data were obtained by the mesh method. When ω's are negative there exist attraction forces between the adsorbed species. Inversely, when ω's are positive there exist repulsive forces between

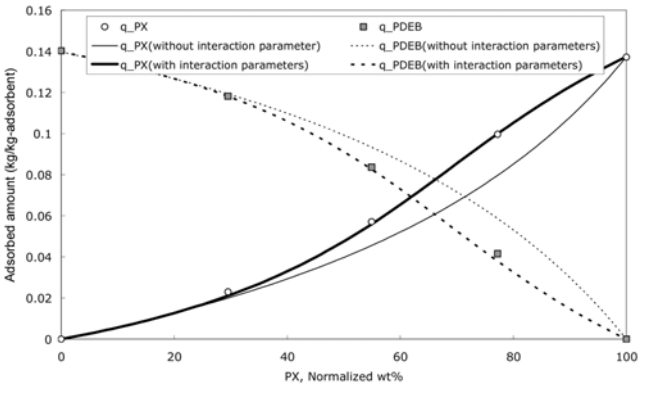

Fig. 7. Equilibrium concentrations of adsorbed liquid phase for a PX-PDEB binary system at various values of equilibrium free liquid phase concentrations of PX. Extended Langmuir isotherm without interaction parameters and modified extended Langmuir isotherm with interaction parameters plotted and compared with the experimental data.

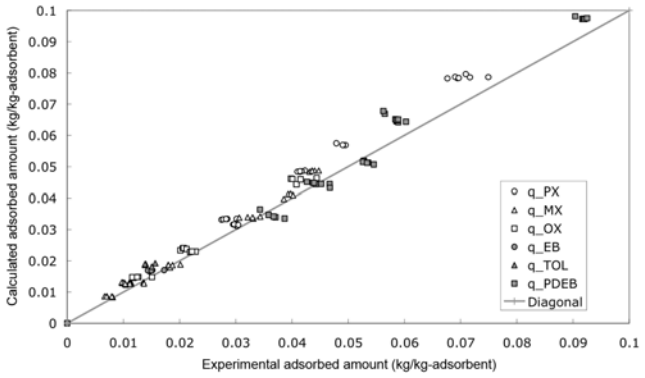

Fig. 8. Comparison between experimental data and multi-component isotherm derived from binary adsorption experiment.

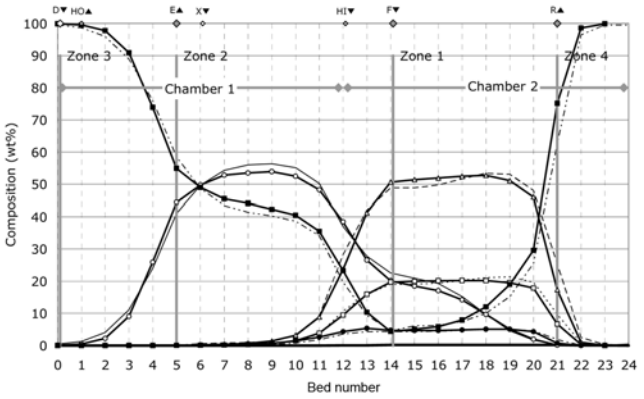

Fig. 9. Comparison of the actual concentration profiles with the simulation result (Empty circle: actual PX; empty triangle: actual MX; empty square: actual OX, filled circle: actual EB; filled square: actual PDEB; ——: calculated PX; ------: calculated MX, ·····: calculated OX; —·—·—·—: calculated EB; —··—··—··—: calculated PDEB).

the adsorbed species. Needless to say, the interaction parameter between the same species ω_{ii} is zero. All of the isotherms, even including the Freundlich isotherm, showed excellent agreement with the experimental data when appropriate interaction parameters were chosen. As shown in Fig. 7, which shows the equilibrium concentrations in the PX-PDEB binary system, a rather big discrepancy was found in the isotherm without interaction parameters.

The interaction parameters obtained from the binary experiment were checked to determine their expandability to a multi-component system with more than three components by comparing the equilibrium concentrations from the experiment with those from the calculation. Among the various isotherms, the Langmuir isotherm showed the closest predictability. Fig. 8 shows a comparison between the experiment and calculation for multi-component adsorption experiments with more than three components. The interaction parameters obtained from the binary experiment turned out to be expandable to a multi-component system with high accuracy. Considering its robustness and stability, the Langmuir isotherm was chosen for simulation and analysis.

SIMULATION RESULTS AND DISCUSSION

The current operation conditions were used to tune the simulation model. The most important operational variables are the zone flow rate ratios, which are defined as the ratios between the liquid flow rate of each zone and an imaginary solid flow rate calculated from the port switching frequency. The other important operational variables are the line flushing rate ratios, which are defined as the ratios between the line flushing flow rates and the volume of the longest bed line. All of the actual flow rates are calculated from these flow rate ratios, designated by an engineer and transferred to and implemented in a computer control system for plant operation.

The recovery and purity of the PX at the extract node are monitored during normal operation as an index for the performance of the adsorption chamber.

$$\text{Recovery} = \frac{Q_E C_{PX,E}}{Q_F C_{PX,F}} = \frac{Q_E C_{PX,E}}{(Q_E C_{PX,E} + Q_R C_{PX,R})} \quad (27)$$

Every few months the concentration profiles of all the species along the bed axis are analyzed to take a closer look at the status of the chamber. After careful parameter tuning using mass transfer coefficients, we could get a recovery and purity of PX that was comparable to actual plant data and get concentration profiles that were in relatively good agreement with the actual profiles as shown in Fig. 9. The value of the mass transfer coefficient obtained was 0.06 m/s. In the course of simulation, different mass transfer coefficients for each SMB zone were used to reflect dispersion effects by different zone flow rates. Each mass transfer coefficient was adjusted to accord with the actual operating results of SMB process. This method is useful with multi-cell models.

Since the SMB is a dynamic process that never gets to the stationary steady state, the PX concentration at the exit of the chamber always fluctuates. Fig. 10 reveals such a fluctuation in PX concentration at the extract stream. The thin and thick lines represent, respectively, the PX concentrations at the inlet and outlet of a bed line used for the extract stream at that moment. As expected, there exists a certain delay for the PX concentration to reach its highest position because a bed line is washed with PDEB just before it is used for the extract stream, as explained previously.

The model, after it was developed and tuned, was used for a further simulation to see whether it could explain some plant problems.

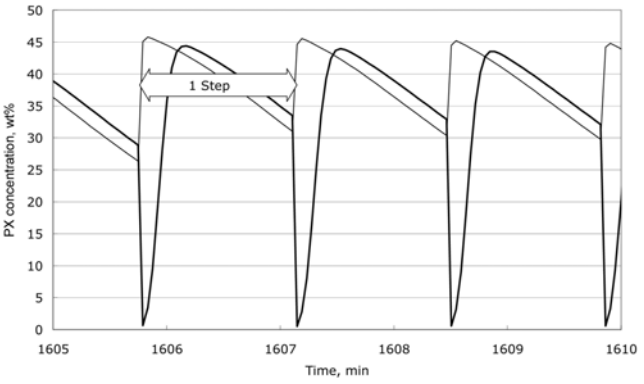

Fig. 10. PX concentrations at extract stream inlet and outlet (thin line: inlet; thick line: outlet).

One of the biggest difficulties in a commercial Parex unit is the increase of pressure drop across the beds. The channeling of liquid flow due to partial coverage of fines on the bed top is believed to be one of the most plausible scenarios for this pressure drop increase. Another candidate for explaining the pressure drop increase is bed compression, which may occur when fine particles penetrate into the bed and therefore reduce the overall bed porosity. Since channeling and bed compression are not that different, despite the quite different mechanisms for increasing the pressure drop, we will focus only on channeling here. The pressure drop across a bed can be calculated by some correlations proposed by Ergun, Chilton and Colburn, and Kozeny [38-40]. Among these correlations Ergun's correlation as expressed in (28) turned out to be the most comparable to the actual data.

$$f=\left(\frac{d_p}{L}\right)\frac{\Delta P}{\rho(\varepsilon_b v)^2}=\left(\frac{1-\varepsilon_b}{\varepsilon_b^3}\right)\left[\frac{150(1-\varepsilon_b)}{Re}+1.75\right] \quad (28)$$

Here f and Re denote the friction factor and Reynolds number, respectively. To quantify the channeling effect, we define the degree of channeling by the fraction of the bed top covered with fines and assume no flow under that fraction, albeit this is an oversimplification. Fig. 11 shows the relationship between the pressure drop and degree of channeling.

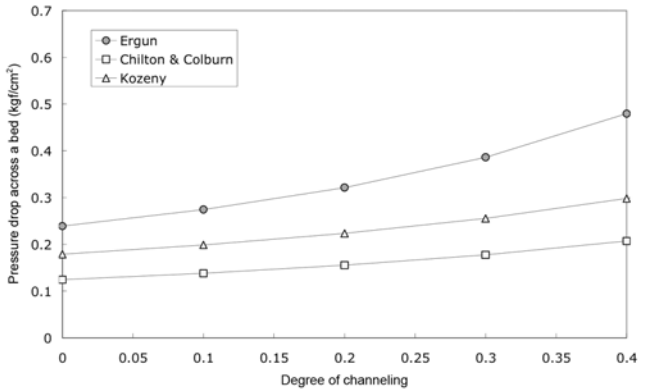

Fig. 11. Pressure drop across a bed belonging to zone 1 at various values for the degree of channeling. The liquid flow is assumed to be zero through a certain portion where the bed top is covered with fines.

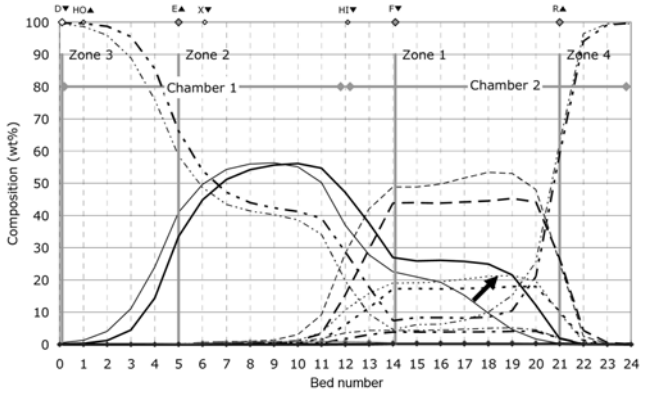

Fig. 12. Effect of channeling on separation performance (Thin lines: 10% degree of channeling; thick lines: 50% degree of channeling. Other symbols are the same as defined for Fig. 9).

In Fig. 12, we compare the concentration profile of a 50% degree of channeling with the normal state, after considering the pressure drop increase in a commercial plant. The interesting thing is that the PX concentration in zone 1 becomes much higher as the degree of channeling increases, which is quite similar to the phenomenon observed when an adsorbent loses its initial capacity. The results found here tell us that one has to search carefully for causes and remedies when chamber separation performance decreases.

When a deterioration in adsorption chamber separation performance is detected, one has to consider many aspects including improper operation conditions, mechanical leaks, flowmeter malfunction, adsorbent hydration, the adsorbent itself, channeling, bed compression and so forth. Based on the analysis of channeling or bed compression, even if they are not directly evident, we surveyed methods that can improve the separation performance. The potential mechanisms of fine formation and methods for removing the fines already in the bed were carefully examined and experimentally verified. After proper treatment on the chamber, separation performance was greatly improved, equivalent to an annual savings of more than 5 billion KRW (Korean Won). The permanent prevention of pressure drop increase is also proposed by the authors [41].

The zone ratios were also changed based on the simulation results, leading to a further increase in the PX production rate. After changing the zone ratio between the imaginary flow rate of the adsorbent micropores and the feed flow rate, as well as adjusting the liquid flow rates inside the chamber, we accomplished a recovery increase of more than 2%, which amounts to more than 1 billion KRW on an annual basis.

The feed composition change, new configuration of the chamber, and substitution of new adsorbent are also expected to be some of the hot topics that can be examined by the simulation model.

CONCLUSIONS

A rigorous multi-cell model was developed to predict the performance of a Parex chamber for PX separation from other xylene isomers. Semi-batch and batch experiments were performed to obtain the equilibrium concentrations of single and binary components respectively. An extended Langmuir isotherm with interaction parameters was proposed and implemented into the model. To avoid the problem of high dimensionality, a cell-by-cell approach was proposed to solve the model. The model parameters were tuned to fit actual plant data and then it was used for applications to commercial plant. The effects of channeling, bed compression, and zone ratio changes were simulated and analyzed. The simulation results were applied successfully to the commercial plant with some practical benefits. The simulation model is expected to contribute to operate condition optimization, trouble shooting, and productivity enhancement linked with the modification of neighboring units including a configuration change.

ACKNOWLEDGMENT

The authors also acknowledge the assistance of Sung Jun Lee of SK Energy and Youn Seok Park, Chang Youl Lee, Je Myung Park,

Pil Jong Cho, Oksoo Kim, Kyeng Su Kim and other colleagues in Samsung Total.

NOMENCLATURE

A : coefficient relating the height equivalent to a theoretical plate [m]
a : mass transfer area [m^2]
B : coefficient relating the height equivalent to a theoretical plate [s^{-1}]
b : constant used in various isotherms, different unit depending on the isotherm used
C : concentration [kg/m^3]
D : axial dispersion coefficient [m^2/s]
d : particle diameter [m]
f : friction factor, $(d_p/L)\ \Delta P/[\rho_l\ (\varepsilon_b v)^2]$
K : equilibrium constant [m^3/kg]
k : mass transfer coefficient [m/s]
L : bed length [m]
m : mass [kg]
N : total number [-]
Q : flowrate [m^3/s]
P : pressure [Pa]
q : adsorbed phase concentration [kg/kg-adsorbent]
Re : Reynolds number $[v\ \rho_l\ d_p/(\varepsilon_b\ \mu)]$
t : time [s]
V : volume [m^3]
v : interstitial velocity [m/s]
w : weight fraction
z : axial direction [m]

Abbreviations and Acronyms

CCR : continuous catalyst regeneration
EB : ethylbenzene
GC : gas chromatography
HETP : height equivalent to a theoretical plate, m
IAST : ideal adsorbed solution theory
LOI : loss on ignition
MX : meta-xylene
ODE : ordinary differential equation
OX : ortho-xylene
PDEB : para-diethylbenzene
PX : para-xylene
SMB : simulated moving bed
TMB : true moving bed
TOL : toluene

Greek Letters:

ε : porosity [m^3/m^3]
ρ : density [kg/m^3]
μ : viscosity [Pa s]

Subscripts and Superscripts

* : equilibrium
0 : initial
a : adsorbed liquid phase
ads : adsorbent
b : bed (inter-particle)
c : crystallite
comp : component
E : extract node of an SMB
F : feed node of an SMB
f : feed to a node
HI : flush in
HO : flush out
i : adsorbable component (when attached to C or q)
i : inlet (when attached to Q)
i : particle number (when attached to V)
j : bed number (1-24)
k : cell number
l : free liquid phase
m : saturation state
o : outlet
p : adsorbent particle
R : raffinate node of an SMB
t : total
X : secondary flush

REFERENCES

1. P. Pang, *Global petrochemical review*, UOP's Korea Technology Seminar, Jejudo (2004).
2. G. Ash, K. Barth, G. Hotier, L. Mank and P. Renard, *Revue De L Institut Francais Du Petrole*, **49**, 541 (1994).
3. D. B. Broughton and C. G. Gerhold, US Patent 2,985,589 (1961).
4. D. B. Broughton, R. W. Neuzil, J. M. Pharis and C. S. Brearley, *Chem. Eng. Prog.*, **66**, 70 (1970).
5. M. M. Kearney and K. L. Hieb, US Patent 5,102,553 (1992).
6. J. Kim, N. Abunasser and P. Wankat, *Korean J. Chem. Eng.*, **22**, 619 (2005).
7. O. Ludemann-Hombourger, M. Bailly and R. M. Nicoud, *Sep. Sci. Technol.*, **35**, 1285 (2000).
8. O. Ludemann-Hombourger, R. M. Nicoud and M. Bailly, *Sep. Sci. Technol.*, **35**, 1829 (2000).
9. H. Schramm, M. Kaspereit, A. Kienle and A. Seidel-Morgenstern, *Chem. Eng. Technol.*, **25**, 1151 (2002).
10. UOP, Parex process, www.uop.com (accessed).
11. D. C. S. Azevedo, S. B. Neves, A. E. Rodrigues, C. L. Cavalcante Jr. and S. P. Ravagnani, *Anais do I Encontro Brasileiro sobre Adsorção,* Fortaleza, 93 (1997).
12. J. Gu, W. Jiang and X. Gu, *J. East China Univ. Sci. Technol.*, **23**, 725 (1997).
13. K. Lee, *Korean J. Chem. Eng.*, **26**, 468 (2009).
14. Y. Lim, *Korean J. Chem. Eng.*, **21**, 836 (2004).
15. C. Migliorini, M. Mazzotti and M. Morbidelli, *AIChE J.*, **45**, 1411 (1999).
16. M. Minceva and A. E. Rodrigues, *Sep. Sci. Technol.*, **38**, 1463 (2003).
17. M. Minceva and A. E. Rodrigues, *Ind. Eng. Chem. Res.*, **41**, 3454 (2002).
18. Z. Tong, Z. Ge and C. Yang, *ACTA PETROLEI SINICA PETROLEUM PROCESSING SECTION*, **11**, 36 (1995).
19. C.-N. Wei, *Diagnosis of manufacturing plant problems through process model parameter update*, International Federation of Automa-

tion Control Conference, Maastricht (1989).
20. R. H. Fowler and E. A. Guggenheim, *Statistical thermodynamics*, Cambridge University Press, Cambridge (1939).
21. E. Glueckauf, *Trans. Faraday Soc.*, **51**, 1540 (1955).
22. G. Guiochon, S. Golshan-Shirazi and A. M. Katti, *Fundamentals of nonlinear and preparative chromatography*, Academic Press, Boston (1994).
23. D. M. Ruthven, *Principles of adsorption and adsorption processes*, Wiley-Interscience (1984).
24. F. Charton and R. M. Nicoud, *J. Chromatography A*, **702**, 97 (1995).
25. U. P. Ernst and J. T. Hsu, *Ind. Eng. Chem. Res.*, **28**, 1211 (1989).
26. J. J. Van Deemter, F. J. Zuiderweg and A. Klinkenberg, *Chem. Eng. Sci.*, **5**, 1 (1956).
27. Grace Davison, Adsorbents for process application, www.grace-davison.com (accessed).
28. D. W. Breck, *Zeolite molecular sieves: Structure, chemistry and use*, John Wiley & Sons, New York (USA) (1974).
29. C. W. Gear, *Numerical initial value problems in ordinary differential equations*, Prentice Hall, Englewood Cliffs (1971).
30. A. L. Myers and W. D. Seider, *Introduction to chemical engineering and computer calculations*, Prentice-Hall Englewood Cliffs, NJ (1976).
31. C. Beauvais, A. Boutin and A. H. Fuchs, *Adsorption-Journal of the International Adsorption Society*, **11**, 279 (2005).
32. I. Langmuir, *J. Am. Chem. Soc.*, **40**, 1361 (1918).
33. R. M. Nicoud, G. Fuchs, P. Adam, M. Bailly, E. Küsters, F. D. Antia, R. Reuille and E. Schmid, *Chirality* NY, **5**, 267 (1993).
34. H. Freundlich, *Colloid and capillary chemistry*, 3rd German Edn. Methuen, London (1926).
35. S. Sips, *J. Chem. Phys.*, **16**, 490 (1948).
36. J. K. Moon, D. K. Keum and W. K. Lee, *Korean J. Chem. Eng.*, **6**, 172 (1989).
37. A. L. Myers and J. M. Prausnitz, *AIChE J.*, **11**, 121 (1965).
38. T. H. Chilton and A. P. Colburn, *Trans. Am. Inst. Chem. Eng.*, **26**, 178 (1931).
39. S. Ergun, *Chem. Eng. Prog.*, **48**, 89 (1952).
40. J. Kozeny, *Sitzungsberichte der Akademie der Wissenschaften in Wien, MATHEMATISCH-naturwissenschaftliche Klasse, Abteilung IIa*, **136**, 271 (1927).
41. J. Lee and N. C. Shin, Korea Patent Korean Patent issued, 0589122 (2006).